Proceedings 10th NUMGE 2023
10th European Conference on Numerical Methods in Geotechnical Engineering
Zdravkovic L, Kontoe S, Taborda DMG, Tsiampousi A (eds)

https://doi.org/10.53243/NUMGE2023-394

Effects of drainage conditions on state parameter inversion from CPTu

K. Boschi[1], L. Monforte[1], M. Arroyo[2], J.M. Carbonell[3], A. Gens[2]

[1]*International Centre for Numerical Methods in Engineering, Barcelona, Spain*
[2]*CIMNE – Universitat Politècnica de Catalunya – BarcelonaTech, Barcelona, Spain*
[3] *Universitat de Vic – Universitat Central de Catalunya (UVic-UCC) – CIMNE, Spain*

ABSTRACT: The state parameter is a key descriptor to understand the potential soil vulnerability to liquefaction. State parameter is often inverted from CPTu readings, but inversion methods have been developed only for fully drained and fully undrained conditions. Therefore, the results are sensitive to partial drainage upon penetration. Cone penetration tests with pore pressure measurements (CPTu tests) in brittle, potentially liquefiable, soils are simulated by means of a code based on the Particle Finite Element Method and adapted for the analysis of fully hydromechanically-coupled geotechnical problems (G-PFEM). The brittle behaviour of the investigated soils is satisfactorily captured by employing the CASM constitutive model and a non-local regularization technique is adopted to prevent the pathological mesh dependence associated with continuum analyses of problems involving softening materials. CPTu tests are simulated for soils characterised by different degree of brittleness, investigating the role played by hydraulic conductivity, and so by various drainage conditions. The availability of a full numerical solution to explore aspects of soil response during penetration, which are not possible when only global CPTu response is available, is exploited.

Keywords: PFEM; hydro-mechanical coupled model; CASM; CPTu tests; brittle soils.

1 INTRODUCTION

A large variety of saturated soils (as loose sands, sensitive or quick clays, mine tailings etc.) may be susceptible to static liquefaction: during undrained loading, the shear strength reaches a peak value and then reduces until attaining a residual one, which can also be significantly lower than the former. Given the momentous consequences of many failures involving this kind of brittle behaviour (Arroyo & Gens, 2021), it is important to identify and characterise the risk. Within the framework of critical state soil mechanics, Been and Jefferies (1985) firstly introduced the concept of state parameter ψ, that is the difference between the current void ratio and the void ratio on the Critical State Line (CSL) at the same value of mean effective stress, as a fundamental descriptor for the soil state to assess its potential to present either a dilative behaviour ($\psi < 0$) or contractive one ($\psi > 0$) and so prone to liquefy.

Since state-preserving extraction of samples from geo-materials susceptible to static liquefaction has proven very difficult (Been, 2016), in situ tests and, above all, cone penetration tests with pore pressure measurements (CPTu tests) are preferred to identify and characterise these materials. Nevertheless, the interpretation of CPTu tests in brittle soils is more uncertain than that in more ductile ones (Karlsrud et al., 2005; Robertson and Cabal, 2014; Monforte et al., 2022). As for ψ prediction, Been et al. (1989) and Plewes et al. (1992) proposed the following expression:

$$Q_p\left(1 - B_q\right) + 1 = k \cdot \exp(-m\,\psi_0) \qquad (1)$$

where $Q_p\left(1 - B_q\right) + 1$ is the normalized effective tip resistance, with $Q_p = (q_c - p_0)/p_0'$ (q_c is the registered cone tip resistance, p_0 and p_0' stand for the initial mean total and effective stress) and excess water pressure ratio B_q, taken by these authors equal to $B_{q2} = \Delta u_2/(q_c - p_0)$ (Δu_2 is the excess pore pressure measured at the cone shoulder). Moreover, ψ_0 is the initial soil ψ value, k and m material dependent parameters. Under fully-drained conditions, k and m were found to be complex functions of various soil properties and few correlations to quantify them were provided (Shuttle & Jefferies, 1998; Robertson, 2009; Shuttle & Jefferies, 2016). Under fully undrained conditions, Plewes et al. (1992), Pezeshki and Ahmadi (2021) and, recently, Monforte et al. (2023) have proposed closed-form solutions to derive k and m. Nevertheless, the effect of partial drainage in predicting ψ_0 from CPTu readings has not still been investigated in literature.

Numerical analyses of CPTu tests (Lu et al., 2004; Nazem et al., 2012; Walker and Yu, 2006; Ceccato et al., 2016; 2017; Gens et al., 2016; Monforte et al., 2017a; 2018a; 2018b) can provide insights into the mechanism underlying the insertion process also contributing to a more rational interpretation of the test results.

In this paper, following on Monforte et al. (2021), this problem has been approached by employing G-PFEM code (Geotechnical code based on the Particle Finite Element Method; numerical model in Section 2). 6 sets of soil parameters representing a wide range of degrees of brittleness and state parameters have been used and a series of numerical simulations of cone penetration under different drainage conditions performed and discussed (Section 3). How the relation between CPTu readings and ψ_0 is affected by partial drainage conditions is finally discussed in Section 4.

2 NUMERICAL MODEL

The employed G-PFEM code (implemented in Kratos Multiphysics; Dadvand et al., 2010; Monforte et al., 2017a) is particularly suitable for problems that involve large displacements and strains, a fully coupled hydro-mechanical formulation and soil/rigid body contacts. It is based on PFEM (Oñate et al., 2004), mainly characterised by a Lagrangian description of the motion, low order finite elements and a constant regeneration of the finite element mesh describing the domain, efficiently introducing new elements in regions where they are specially required. The soil domain is discretized with mixed stabilized linear triangles, having displacements, Jacobian and water pressure as degrees of freedom, in order to both alleviate volumetric locking and enhance smoother cone resistance/water pressure curves (Monforte et al., 2017b). Moreover, dealing with brittle soils, to alleviate the mesh-dependency of the solution due to strain-softening, the non-local regularization technique described in Monforte et al. (2019a) is adopted.

The penetration of a smooth cone (radius R = 17.84 mm and apex angle $\alpha = 60°$) is simulated employing an axisymmetric model (shown in Figure 1). The cone is initially whished-in-place at a depth of $11 \cdot R$ and it is pushed at standard velocity v of 0.02 m/s. Null displacements are prescribed at the bottom boundary, whereas null radial displacements at the vertical ones. Initial effective vertical σ'_{v0} and horizontal stresses are imposed to be equal to 100 kPa and 60 kPa, respectively, i.e. K_0 = 0.6, while initial pore pressure u_0 is assumed to be nil. Drainage is only allowed through bottom and top boundaries of the domain. A vertical load q is prescribed at the top boundary to be in equilibrium with $\sigma'_{v0} + u_0$.

Within the framework of large-strain elasto-plasticity, the constitutive model employed is a modified version of the isotropic, critical state-based model CASM (Clay And Sand Model; Mánica el al., 2021; 2022), originally proposed by Yu (1998). The elastic part is described by means of an hyperelastic law in which the bulk modulus depends on mean effective stress p'. A wide variety of yield surface shapes can be obtained for various n and r constitutive parameter values, this latter controlling the vertical distance between isotropic compression line ICL and CSL (assumed to be straight and parallel). Finally, the non-associated flow rule proposed by Mánica (2021) is adopted.

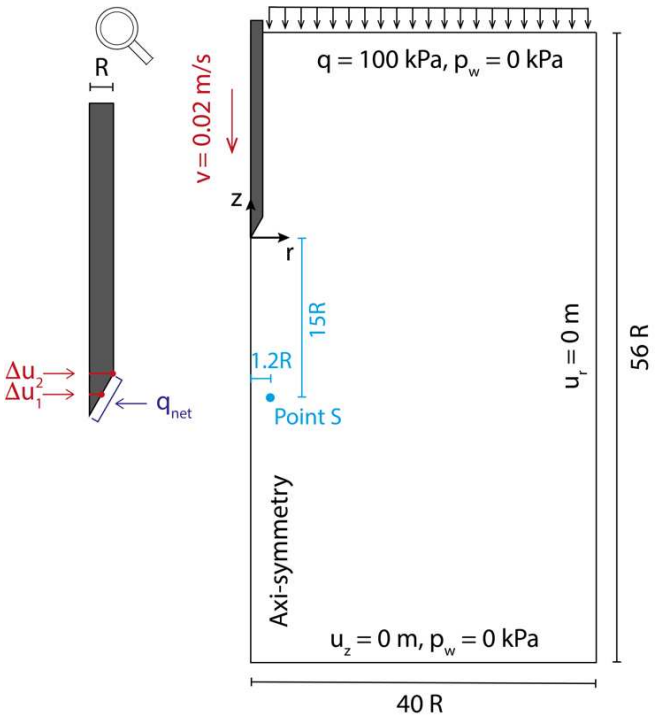

Figure 1. Simulation of CPTu tests: geometry, imposed boundary conditions and measurement locations for pore pressures and net cone tip resistance.

Table 1. Constitutive parameters n and r of the modelled soils, initial state parameter, residual undrained shear strength and brittleness index.

Material	n	r	ψ_0	$S_{u,res}$ [kPa]	I_b
A	4	2	0.023	22	0.07
B	6	2.5	0.033	19	0.22
C	8	4	0.051	13	0.45
D	9	6	0.066	10	0.58
E	10	8	0.077	8	0.66
F	10	12	0.092	6	0.74

Six sets of soil constitutive parameters are employed, associated to the same ICL, but different CSLs and ψ_0. For all the normally-consolidated soils modelled, Poisson's modulus ν is equal to 0.3, shear modulus G = 4.2 MPa, void ratio belonging to ICL at p' = 100 kPa e_0 = 1, slope of CSL in the $ln(p')$ - e space λ = 0.053, slope of the reloading curve in the same plane k = 0.016, slope of CSL in the p'- q plane M = 0.98 and flow rule model parameter m = 2.5 (Monforte et al., 2021). In Table 1,

the different n, r and so ψ_0 values are listed for each soil. Analogously to what done by Monforte et al. (2021), performing undrained triaxial tests with initial stress state of the simulated specimens equal to the one that is used in the cone penetration simulations, peak shear strength $S_{u,peak}$ around 24 kPa and residual $S_{u,res}$ values listed in Table 1 are derived, resulting in different brittleness indexes $I_b = 1 - S_{u,res} / S_{u,peak}$.

3 NUMERICAL RESULTS

Cone penetration into the 6 soil materials of Table 1 is simulated by considering a smooth cone/soil interface (as described in Monforte et al., 2021).

To observe the behaviour for different drainage conditions, different values of hydraulic conductivity K, ranging between 10^{-9} and 10^{-4} m/s, are investigated (for this aim, different cone penetration rates could have been also used). In Figure 2, profiles, with respect to normalised penetration depth z/R, of net cone tip resistance q_{net} (equal to $q_c - \sigma'_{v0} - u_0$) and excess pore pressure measured at the cone midface Δu_1 are shown for some representative numerical tests. It can be observed that, for all materials and drainage conditions, a clear steady state is observed after a penetration not larger than $8R$. Table 2 shows steady state values of the main cone penetration parameters (q_{net}, Δu_1 and Δu_2) obtained in different analyses (Material A, C, E and F for K = 10^{-5}, $5 \cdot 10^{-7}$, 10^{-9} m/s).

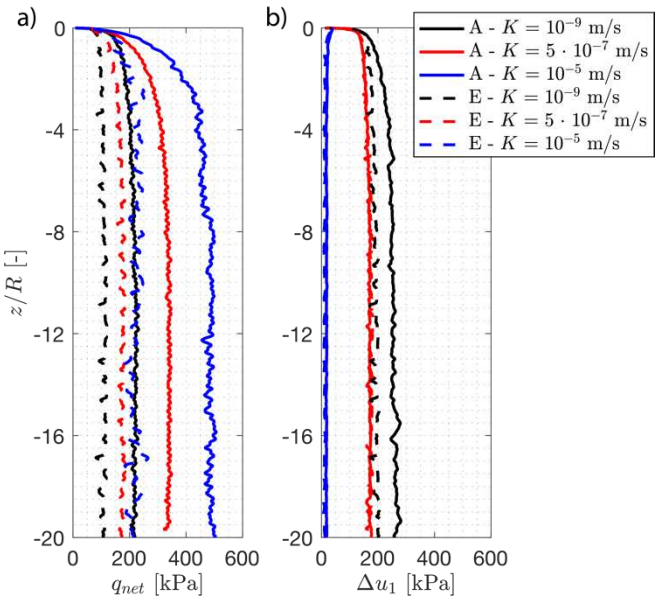

Figure 2. Results as a function of normalised cone penetration depth z/R: a) net cone tip resistance q_{net}, b) excess pore pressure measured at the cone tip Δu_1.

According to Monforte et al. (2021), independently of brittleness, partially drained conditions are observed for normalized cone velocities

$$V_c = \frac{v\,D}{c_v} = \frac{\lambda\,\gamma_w\,v\,D}{\sigma'_{v0}\,(1+e_0)\,K} \qquad (2)$$

ranging between 0.2 and 200 (D is the cone diameter, c_v the in-situ coefficient of consolidation, γ_w the water weight per unit volume). Using this criterion, drained conditions are identified for $K > 10^{-5}$ m/s (in Figure 2 and Table 2); indeed, steady state pore pressures are negligible and q_{net} does not vary with K. Constant steady state q_{net} and pore pressure values are once again obtained for $K < 10^{-8}$ m/s, corresponding to undrained conditions (in Figure 2 and Table 2, cases for $K = 10^{-9}$ m/s). Thus, a range of more or less three orders of magnitude refers to partially drained conditions (in Figure 2 and Table 2, reported cases for $K = 5 \cdot 10^{-7}$ m/s).

Table 2. Results of cone penetration test simulations.

Material	K [m/s]	V_c [-]	q_{net} [kPa]	Δu_1 [kPa]	Δu_2 [kPa]
A	$1 \cdot 10^{-5}$	$2 \cdot 10^{-1}$	486	18	13
	$5 \cdot 10^{-7}$	4	339	170	102
	$1 \cdot 10^{-9}$	$2 \cdot 10^{3}$	220	251	205
C	$1 \cdot 10^{-5}$	$2 \cdot 10^{-1}$	329	15	11
	$5 \cdot 10^{-7}$	4	242	178	121
	$1 \cdot 10^{-9}$	$2 \cdot 10^{3}$	161	223	183
E	$1 \cdot 10^{-5}$	$2 \cdot 10^{-1}$	220	11	7
	$5 \cdot 10^{-7}$	4	176	175	129
	$1 \cdot 10^{-9}$	$2 \cdot 10^{3}$	120	195	164
F	$1 \cdot 10^{-5}$	$2 \cdot 10^{-1}$	194	12	8
	$5 \cdot 10^{-7}$	4	143	172	131
	$1 \cdot 10^{-9}$	$2 \cdot 10^{3}$	95	174	143

Even if all the materials have the same $S_{u,peak}$, under undrained conditions, brittleness index I_b has a very strong influence on the results. Δu tends to increase for lower I_b. However, the major I_b effect concerns q_{net}, which varies from 220 kPa (Material A, less brittle) to 95 kPa (Material F, more brittle).

Increasing K values and so moving towards firstly partially drained conditions and then fully drained ones, Δu turns out to be almost independent of I_b. Nevertheless, a more surprising results is that the differences in q_{net} induced by different undrained brittleness index I_b are not just maintained, but enhanced all the way to fully drained conditions. Despite having the same void ratio, the same initial stress state and the same angle of drained shearing resistance, soils with higher undrained brittleness index I_b and higher initial state parameter ψ_0 show lower tip resistances.

3.1 ψ_0 effect in fully-drained behaviour

Taking advantage of the ability of G-PFEM to perform a realistic simulation of the cone penetration, a more detailed examination of the mechanism underlying the ψ_0 effect under fully-drained conditions is performed.

More precisely, this effect is explored comparing results of tests with Materials A, C, E and F and $K = 10^{-5}$ m/s, in terms of stress, hardening parameter and void ratio evolutions of one individual point (Point S; Figure 1).

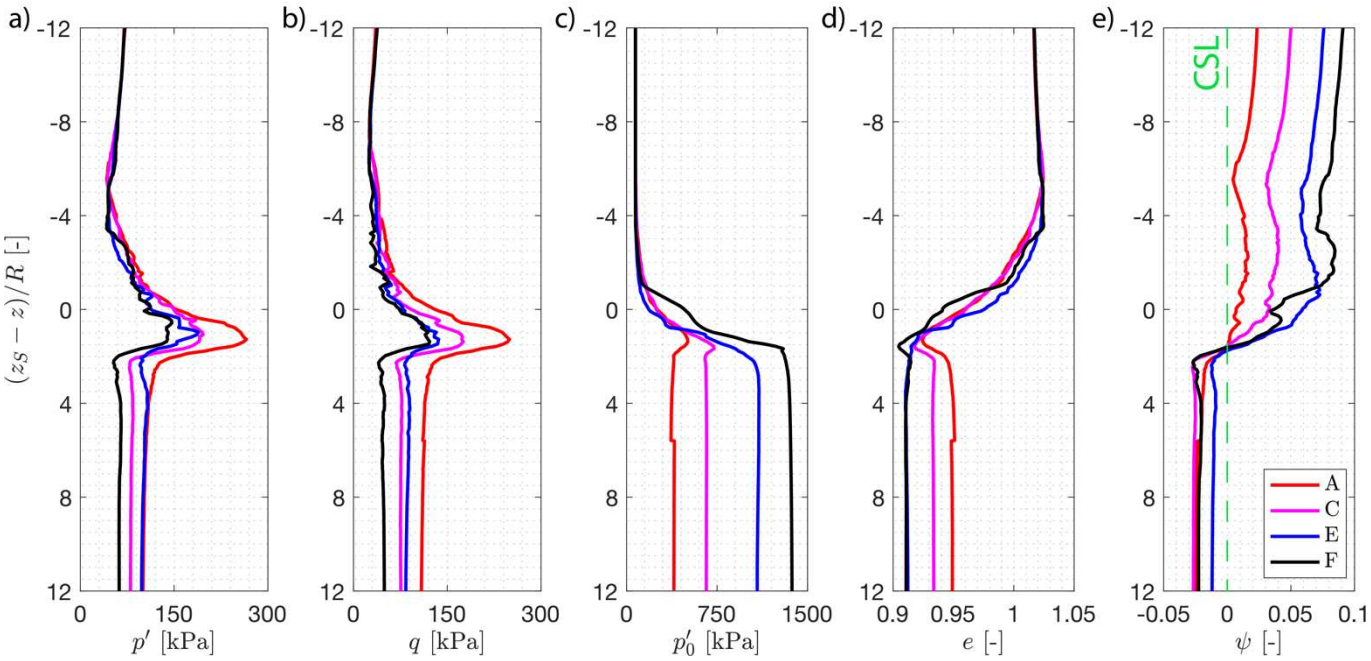

Figure 3. Variation of a) mean effective stress, b) deviatoric stress, c) hardening parameter, d) void ratio and e) state parameter with normalised depth of penetration for Point S (Figure 1). K = 10^{-5} m/s, smooth cone with Materials A, C, E and F.

This point is taken at a radial distance from the cone shaft axis of 1.2R, i.e. located quite close to the soil/shaft contact as soon as the cone tip reaches its level (z_S = *-15R*). The observation point does not coincide with a Gauss point, so information is interpolated from the nearest ones. Figure 3 illustrates, for the different tests, the evolutions of mean effective stress *p'*, deviatoric stress *q*, hardening parameter p'_0 (i.e. the isotropic yield stress), void ratio *e* and state parameter ψ referred to Point S as cone penetration proceeds. The value of zero penetration on the vertical axis, i.e. $(z_S - z)/R = 0$, corresponds to the time when the cone tip reaches the Point S level. Under steady state conditions, these time evolutions are analogous to spatial ones for a fixed time instant and points belonging to a vertical line at a radial distance from the cone shaft axis of 1.2*R*.

From a qualitative point of view, the overall behaviour is the same independently of ψ_0. As soon as Point S starts being affected by the cone penetration, the stress state (*p'* and *q*; Figures 3a and 3b) slightly reduces until the cone tip is a few radii above Point S (approximately 5*R*). Afterwards, the peak in both *p'* and *q* is rapidly reached just after the cone reaches Point S level $(z_S - z)/R \cong 1\text{-}1.2$, together with the achievement of critical state (CS; $\psi = 0$ in Figure 3e). Subsequently, deviatoric and effective mean stresses reduce markedly. Simultaneously (Figure 3c), just before the cone reaches Point S, p'_0 starts increasing, as the soil is in a hardening regime, until the stress state peak is reached; then, p'_0 remains approximately constant. In terms of *e* (Figure 3d), in accordance with the stress state, the evolution is characterised by an initial slight dilatant behaviour, followed by a contractive one with a significant reduction in *e*, only partially recovered during the subsequent unloading. The correspondent passage from $\psi > 0$ before reaching CS to $\psi < 0$ is also shown in Figure 3e.

From a quantitative point of view, however, there is a significant dependence on the tested materials (Table 1), differing in *n* and *r* parameters and so in distance between initial stress state and CSL, i.e. ψ_0, as well as in yield surface shape. Above all, as the ψ_0 of soil increases, a lower peak in the stress state is reached along with a more marked hardening response. The *e* recovered after the cone penetration perturbation is higher for lower ψ_0. The higher steady state q_{net} values obtained for less brittle soils under drained conditions (Figure 2 and Table 2) are associated with the higher peak in the stress state observed for less brittle soils just after being reached by the cone tip (Figures 3a and 3b).

4 STATE PARAMETER INVERSION AND PARTIAL DRAINAGE

Several authors (Been et al. 1985; Been et al. 1989; Shuttle & Jefferies, 2016) have already studied the ψ_0 dependence upon measured q_c under both fully-drained conditions and fully-undrained ones. There have been fewer studies of what happens under partially drained conditions, although some empirical methods (Plewes et al. 1992) are used. An investigation on this subject is

performed in this section based on the results of the numerical cone penetration tests described in Section 3. More precisely, Figure 4 shows these results (symbols) in terms of normalized effective tip resistance $Q_p(1 - B_q) + 1$ evolution as a function of ψ_0, in which a logarithmic scale is used along the y axis and, following Monforte et al. (2023), B_q is taken equal to $B_{q1} = \Delta u_1/(q_c - p_0)$. Different symbols are associated to different K values (and hence to V_c ones as well), whereas the fill colour indicates the corresponding B_{q1} value.

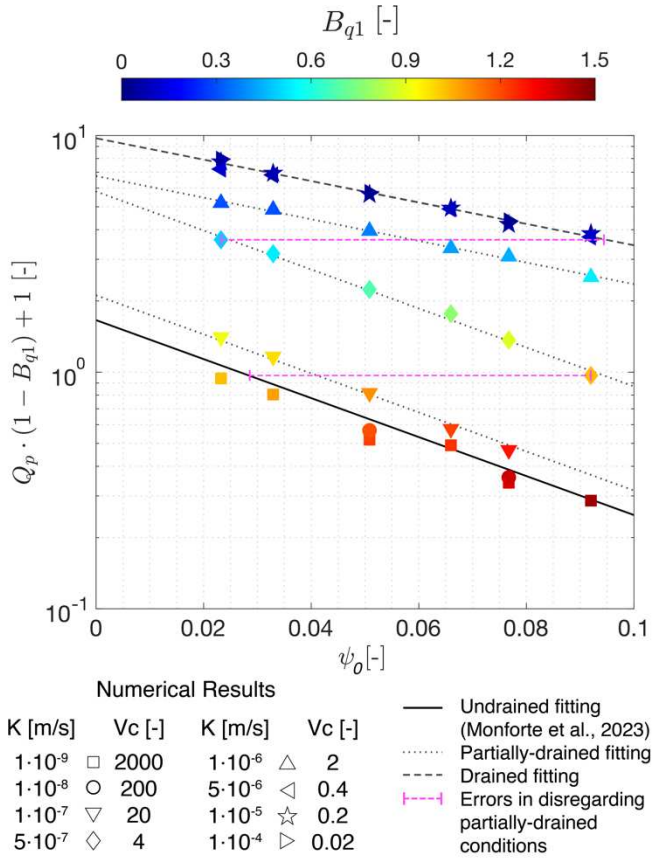

Figure 4. Normalized effective tip resistance vs. state parameter; effect of drainage conditions.

In this plane, all the results associated with a constant V_c value can be fitted by a straight line, i.e. by Equation 1 in this case with $B_q = B_{q1}$, also for partially drained conditions. For $V_c > 200$ (undrained conditions), associated to B_{q1} values > 1, the numerical results turn out to be satisfactorily fitted by employing the closed-form solutions for k and m values (reported in Table 3) derived by Monforte et al. (2023; solid black line), i.e. $m = 1/\lambda$ and $k = 1 + 2/3 \cdot M$ (this latter expression applies to smooth cones). Lowering the V_c value, the k parameter, required to fit the numerical results, starts increasing, followed soon by a reduction in m parameter. For $V_c <$ 0.4 as well as $B_{q1} < 0.1$, all the numerical results can be fitted by a unique line, i.e. the one associated to fully-drained conditions. In Table 3, the fitting k and m parameter values for the investigated V_C values are reported.

Then, as evident from Figure 4, drainage conditions play a key role in predicting ψ_0 from the measured normalized effective tip resistance and neglecting partial drainage conditions would lead to totally unreliable predictions for a wide range of V_c, i.e. 3 orders of magnitude. Figure 4 highlights, through pink lines, some of the most critical gaps between actual ψ_0 parameters and predicted ones if only fully drained or undrained fittings are considered. In case of V_c = 4, if Monforte et al. (2023) expression is employed to predict ψ_0, an underestimation of 70% would be encountered. Conversely, if low B_{q1} values are obtained and the expression for fully-drained conditions is adopted, a massive overestimation would result (for instance up to 300% at ψ_0 = 0.023).

Table 3. k and m parameter values: derived by Monforte et al. (2023) for $V_c \geq 200$, from numerical result fitting for $V_c < 200$.

Drainage Conditions	***V_c***	***k***	***m***
Fully Undrained	2000	1.66	18.87
Fully Undrained	200	1.66	18.87
Partially Drained	20	2.12	18.87
Partially Drained	4	5.87	18.87
Partially Drained	2	6.75	10.42
Partially Drained	0.4	9.60	10.42
Fully Drained	0.2	9.75	10.42
Fully Drained	0.02	9.75	10.42

5 CONCLUSIONS

The performed simulations consider (i) the actual geometrical conditions encountered in cone testing, (ii) constitutive models capable of describing the response of brittle materials characterised by different state parameters and (iii) different drainage conditions by means of a fully hydro-mechanical coupled formulation.

After discussing the obtained CPTu readings (steady state values of net cone tip resistance and excess pore water pressures) as a function of degree of brittleness, the key role played by drainage conditions in the prediction of state parameter, a key descriptor to understand the potential soil vulnerability to liquefaction, from CPTu readings, is demonstrated and quantified for different normalized cone velocities. The need for correctly establishing the drainage condition of the test for interpretation is evident. This could be made through dissipation tests or, more advantageously, through on-the-fly measurements (Monforte et al. 2018b).

Interpretation of CPTu test results is crucial for liquefaction risk assessment. However, this is not a task exempt of uncertainties, especially for non-standard soils such as brittle ones. The application of advanced numerical modelling, by means of G-PFEM, for full

field cone penetration test simulation seems to offer good chance to advance in this respect.

6 ACKNOWLEDGEMENTS

Financial support of Spain Research Agency (MCIN/AEI/10.13039/501100011033) through the Severo Ochoa Centre of Excellence project (CEX2018-000797-S) and research project PID2020-119598RB-I00.

7 REFERENCES

Arroyo, M., & Gens, A. (2021). Computational analyses of Dam I failure at the Corrego de Feijao mine in Brumadinho; available at http://www.mpf.mp.br/mg/sala-de-imprensa/docs/2021/relatorio-final-cinme-upc-1.

Been, K., & Jefferies, M.G. (1985). A state parameter for sands. Géotechnique, 35:99-112.

Been, K., Crooks, J. H. A., & Jefferies, M. G. (1989). Interpretation of material state from the CPT in sands and clays. In Penetration testing in the UK (pp. 215-218). Thomas Telford Publishing.

Been, K. (2016). Characterizing mine tailings for geotechnical design. Australian Geomechanics, 51(4), 59-78.

Ceccato, F., Beuth, L., Vermeer, P.A., Simonini, P. (2016). Two-phase Material Point Method applied to the study of cone penetration. Comput. Geotech. 80, 440–452.

Ceccato, F., Simonini, P. (2017). Numerical study of partially drained penetration and pore pressure dissipation in piezocone test. Acta Geotech. 12, 195–209.

Dadvand, P., Rossi, R., Oñate, E., (2010). An object-oriented environment for developing finite element codes for multidisciplinary applications. Arch. Comput. Methods Eng. 17 (3), 253–297.

Gens, A., Arroyo, M., Butlanska, J., Carbonell, J.M Ciantia, M., Monforte, L., O'Sullivan, C. (2016). Simulation of the cone penetration test: discrete and continuum approaches, Australian Geomechanics 51, 169-182.

Karlsrud, K., Lunne, T., Kort, D. A., & Strandvik, S. (2005). CPTU correlations for clays. In Proceedings of the 16th interna-tional conference on soil mechanics and geotechnical engi-neering (pp. 693-702). IOS Press.

Lu, Q., Randolph, M.F., Hu, Y., Bugarski, I.C., (2004). A numerical study of cone penetration in clay. Géotechnique 54 (4), 257–267.

Mánica, M.A., Arroyo, M., Gens, A. (2021). Effects of tailings viscosity on liquefaction triggering analyses, Tailings and Mine Waste conference.

Mánica, M.A., Arroyo, M., Gens, A., and Monforte, L. (2022). Application of a critical state model to the Merriespruit tailings dam failure. Proceedings of the Institution of Civil Engineers – Geotechnical Engineering, 175(2):151-165.

Monforte, L., Arroyo, M., Carbonell, J.M., Gens, A. (2017a). Numerical simulation of undrained insertion problems in geotechnical engineering with the particle finite element method (PFEM). Comput. Geotech. 82, 44–156.

Monforte, L., Carbonell, J.M., Arroyo, M., Gens, A. (2017b). Performance of mixed formulations for the particle finite element method in soil mechanics problems. Computational Particle Mechanics 4, 269–284.

Monforte, L., Arroyo, M., Carbonell, J.M., Gens, A. (2018a). Coupled effective stress analysis of insertion problems in geotechnics with the Particle Finite Element Method. Comput. Geotech. 101, 114–129.

Monforte, L., Arroyo, M., Gens, A., Carbonell, J.M. (2018b). Hydraulic conductivity from piezocone on-the-fly: a numerical evaluation. Géotechnique Letters 8 (4), 268–277.

Monforte, L., Ciantia, M.O., Carbonell, J.M., Arroyo, M., Gens, A., (2019a). A stable mesh-independent approach for numerical modelling of structured soils at large strains. Comput. Geotech. 116, 103215.

Monforte, L., Gens, A., Arroyo, M., Mánica, M., & Carbonell, J. M. (2021). Analysis of cone penetration in brittle liquefiable soils. Computers and Geotechnics, 134, 104123.

Monforte, L., Arroyo, M., & Gens, A. (2022). Undrained strength from CPTu in brittle soils: A numerical perspective. In Cone Penetration Testing 2022 (pp. 591-597). CRC Press.

Monforte, L., Arroyo, M., Gens, A. (2023). A relation between cone metrics and the state parameter for liquefiable soils. *Under review*

Nazem, M., Carter, J.P., Airey, D.W., Chow, S.H. (2012). Dynamic analysis of a smooth penetrometer free-falling into uniform clay. Géotechnique 62, 893–905.

Oñate, E., Idelsohn, S.R., Del Pin, F., Aubry, R. (2004). The particle finite element method - an overview. Int. J. Comput. Methods 1 (02), 267–307.

Pezeshki, A., & Ahmadi, M.M. (2021). In situ state of tailing silts using a numerical model of piezocone penetration test developed by Norsand model. International Journal of Geomechanics.

Plewes, H.D., Davies, M.P., & Jefferies, M.G. (1992). CPT based screening procedure for evaluating liquefaction susceptibility. In Proceedings of the 45th Canadian geotechnical Conference, Toronto, Canada.

Robertson, P. K. (2009). Interpretation of cone penetration tests—a unified approach. Canadian geotechnical journal, 46(11), 1337-1355.

Robertson, P.K., & Cabal, K.L. (2014). Guide to Cone penetration testing for Geotechnical Engineering.

Shuttle, D., & Jefferies, M. (1998). Dimensionless and unbiased CPT interpretation in sand. International Journal for Numerical and Analytical Methods in Geomechanics, 22(5), 351-391.

Shuttle, D., & Jefferies, M. (2016). Determining silt state from CPTu. Geotechnical Research 3(3):90-118.

Walker, J., Yu, H.S. (2006). Adaptive finite element analysis of cone penetration in clay. Acta Geotech. 1, 43–57.

Yu, H.S. (1998). CASM: A unified state parameter model for clay and sand. International Journal for Numerical and Analytical Methods in Geomechanics 22, 621–653.